Femtosecond Carotenoid to Retinal Energy Transfer in Xanthorhodopsin

Tomáš Polívka,[†‡*] Sergei P. Balashov,[§] Pavel Chábera,[†] Eleonora S. Imasheva,[§] Arkady Yartsev,[¶] Villy Sundström,[¶] and Janos K. Lanyi[§]

[†]Institute of Physical Biology, University of South Bohemia, Nové Hrady, Czech Republic; [‡]Institute of Plant Molecular Biology, Biological Center, Czech Academy of Sciences, České Budějovice, Czech Republic; [§]Department of Physiology and Biophysics, University of California, Irvine, California; and [¶]Department of Chemical Physics, Lund University, Lund, Sweden

ABSTRACT Xanthorhodopsin of the extremely halophilic bacterium *Salinibacter ruber* represents a novel antenna system. It consists of a carbonyl carotenoid, salinixanthin, bound to a retinal protein that serves as a light-driven transmembrane proton pump similar to bacteriorhodopsin of archaea. Here we apply the femtosecond transient absorption technique to reveal the excited-state dynamics of salinixanthin both in solution and in xanthorhodopsin. The results not only disclose extremely fast energy transfer rates and pathways, they also reveal effects of the binding site on the excited-state properties of the carotenoid. We compared the excited-state dynamics of salinixanthin in xanthorhodopsin and in $NaBH_4$-treated xanthorhodopsin. The $NaBH_4$ treatment prevents energy transfer without perturbing the carotenoid binding site, and allows observation of changes in salinixanthin excited-state dynamics related to specific binding. The S_1 lifetimes of salinixanthin in untreated and $NaBH_4$-treated xanthorhodopsin were identical (3 ps), confirming the absence of the S_1-mediated energy transfer. The kinetics of salinixanthin S_2 decay probed in the near-infrared region demonstrated a change of the S_2 lifetime from 66 fs in untreated xanthorhodopsin to 110 fs in the $NaBH_4$-treated protein. This corresponds to a salinixanthin-retinal energy transfer time of 165 fs and an efficiency of 40%. In addition, binding of salinixanthin to xanthorhodopsin increases the population of the S* state that decays in 6 ps predominantly to the ground state, but a small fraction (<10%) of the S* state generates a triplet state.

INTRODUCTION

Light harvesting is a vitally important process for photosynthetic organisms because it provides the means to maintain the rates of photochemical reactions that convert solar energy into other kinds of directly exploitable energy. The light-harvesting complexes exhibit large structural and spectral variability across a variety of photosynthetic systems (1). In the majority of these systems, the antenna function is carried out by two types of pigments, (bacterio)chlorophylls and carotenoids, whose excited-state properties and energy transfer efficiencies have been the subject of numerous experimental and theoretical studies (2–4). In higher plants the role of carotenoids is predominantly to provide photoprotection; however, in microorganisms their light-harvesting function is more important, and in some systems carotenoids are the major light-harvesting pigments (5).

The much simpler retinal-based energy transducers of the archaea, bacteriorhodopsin and archaerhodopsin, lack antennae. Absorption of light and the proton transport it drives take place within one protein molecule containing a single retinal chromophore. These proteins undergo a cycle of reactions that span a time domain from femtoseconds to milliseconds, resulting in the translocation of a proton from inside the cell to the outside and the generation of a transmembrane potential that is usable for ATP synthesis, ion transport, and cell motility. The reaction is initiated by the light-induced isomerization of the chromophore from all-*trans* to 13-*cis* (6) and involves changes in the pK_a values of the buried carboxyl groups (7), and small-scale (8) and large-scale (9) conformational changes of the protein. The early events involve spectral evolution, which has been interpreted as relaxation through a series of excited states and photoproducts (denoted as H, I, and J (10–14)) that leads to formation of the 13-*cis* photoproduct K (15).

Only a few genes—those coding for the retinal protein (opsin) and the enzymes in retinal synthesis—are needed to support this apparently very ancient type of phototrophy. The simplicity of such a light-energy transducing system apparently explains the wide spread of retinal protein genes in the genomes of not only archaea but also, as is now known, the many different families of eubacteria and eucaryotes. Some are pumps and some are sensors. More than 2500 different opsin genes have been identified, but only a few of the proteins have been isolated from cultured organisms (16). Among them, one retinal protein, xanthorhodopsin (17), from the cell membrane of extremely halophilic eubacterium *Salinibacter ruber* (18), showed an unexpected association with a C40 carotenoid, salinixanthin (19). This carotenoid was found to undergo large reversible absorption changes when the retinal chromophore was removed and replaced in the protein (17). The carotenoid is bound to the protein in a 1:1 ratio. The action spectrum for proton transport indicated that light absorbed not only by the retinal but also by the carotenoid is utilized for proton transport, with ~40% efficiency (17). Subsequent studies using steady-state

Submitted October 27, 2008, and accepted for publication January 8, 2009.

*Correspondence: polivka@ufb.jcu.cz

Editor: Enrico Gratton.

0006-3495/09/03/2268/10 $2.00

doi: 10.1016/j.bpj.2009.01.004

fluorescence measurements demonstrated that there indeed exists an efficient energy-transfer channel between salinixanthin and retinal (20), making xanthorhodopsin the simplest antenna protein known so far.

The recently resolved crystal structure of xanthorhodopsin (21) shows that the two chromophores are at a 46° angle and the distance between their centers is 11.7 Å (see the Supporting Material). The ring of the carotenoid is turned 82° from the plane of the polyene chain and immobilized in the binding site within 5 Å from the ionone ring of retinal. This explains both the well-resolved structured absorption spectrum of the bound salinixanthin (Fig. 1) and its dependence on retinal (22), which constitutes part of its binding site.

The light-harvesting function of carotenoids is well documented in many photosynthetic systems, but the precise mechanisms of energy transfer involving carotenoids are less understood than those involving (bacterio)chlorophylls. This is mainly because of the complex excited-state structure of carotenoids. The strong absorption of carotenoids in the blue-green spectral region is caused by a transition to the excited state, called S_2 ($1B_u^+$ in the C_{2h} symmetry group notation). For symmetry reasons, the transition to the lowest excited state, S_1 ($1A_g^-$), from the ground state is forbidden, but the S_1 state is populated via S_2-to-S_1 internal conversion on a timescale of a few hundred femtoseconds (2). Both S_2 and S_1 states were identified as energy donors in carotenoid-(bacterio)chlorophyll antenna systems (2–4,23). Moreover, new experimental approaches in the past 5 years also revealed that the generally accepted dual-excited-states (S_1 and S_2) scheme is a simplification, because more dark states may be located between (or in close vicinity of) the S_1 and S_2 states, making the excited-state dynamics vastly complicated (2,24,25). These excited states, called $1B_u^-$, $3A_g^-$ (24), and S* (26), become more important for carotenoids with longer conjugated chains. For carotenoids with conjugation length $N > 11$, all of these states could lie between the S_2 and S_1 states (2,24), making them all potential energy donors in the energy transfer process. Moreover, recent studies on carotenoids containing a conjugated carbonyl group disclosed another dimension in the complex pattern of excited-state dynamics: the spectroscopic properties of these carotenoids exhibit a strong dependence on the polarity of the environment, which is attributed to the presence of an intramolecular charge transfer (ICT) state (27–29).

In xanthorhodopsin, the lowest excited state of the retinal chromophore is too high to allow for energy transfer from the S_1 state of salinixanthin. Consequently, a salinixanthin-to-retinal energy transfer was suggested to occur exclusively from the salinixanthin S_2 state (17). Despite the evidence for salinixanthin-to-retinal energy transfer indicated by fluorescence excitation spectra and carotenoid fluorescence changes (20), direct time-resolved methods are necessary to determine the energy transfer rates and verify the energy transfer pathway(s). Salinixanthin has 13 conjugated double bonds (11 linear C=C, plus C=C and C=O at the terminal ring), and thus some dark states located in the S_2-S_1 gap may have energies favorable for energy transfer. Moreover, salinixanthin contains a conjugated carbonyl group that may activate the ICT state. Here we apply the femtosecond transient absorption technique to reveal the excited-state dynamics of salinixanthin both in solution and in xanthorhodopsin. The results reveal not only extremely fast energy transfer rates and pathways, but also the effects of the binding site on the excited-state properties of salinixanthin.

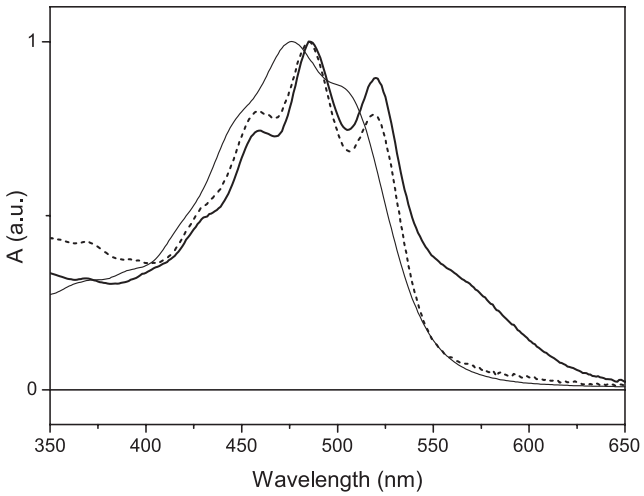

FIGURE 1 Absorption spectra of cell membrane fraction containing xanthorhodopsin (*thick solid line*), the same membrane after treatment with $NaBH_4$ (*dashed line*), and salinixanthin in methanol (*thin solid line*).

MATERIALS AND METHODS

Sample preparation

Cultures of *Salinibacter ruber*, strain M31, were grown in the medium described in Imasheva et al. (30). The cells were collected by centrifugation and subjected to overnight dialysis versus water (17). The fraction of cell membranes enriched in xanthorhodopsin was obtained as previously described (22). The pH was adjusted to 7.8 using 10 mM HEPES as a buffer. Reduction of the retinal Schiff base C=N double bond to a single bond with $NaBH_4$ was performed at pH 8 under illumination at 550–650 nm for 1 h as previously described (20). The concentration of $NaBH_4$ was 5 mg/mL. Salinixanthin was extracted from cell membranes containing xanthorhodopsin using an acetone/methanol (7:3) mixture, and purified by precipitating phospholipids with cold acetone and removing them by centrifugation as previously described (19).

Femtosecond transient absorption

For measurement in the visible spectral region, femtosecond pulses were obtained from a 1 kHz femtosecond laser system (Integra-I, Quantronix, East Setauket, NY). The output pulses had a ~130 fs width, an average energy of ~2 mJ/pulse, and a central wavelength of 780 nm. The pulses were divided into two paths: one to pump an optical parametric amplifier (TOPAS, Light Conversion, Vilnius, Lithuania) for generation of excitation pulses, and the other to produce white-light continuum probe pulses in a 0.3 cm sapphire plate. For signal detection, the probe beam and an identical

reference beam were focused onto the entrance slit of a spectrograph, which then dispersed both beams onto a dual photodiode array detection system (ExciPro, CDP Systems, Moscow, Russia). A 1-mm pathlength rotating quartz cuvette spinning at a rate to ensure that each excitation pulse hit a fresh sample was used for measurements. The intensity of excitation was 2×10^{14} photons · pulse^{-1} · cm^{-2}. The mutual orientation of the excitation and probe beams was set to the magic angle (54.7°).

For single-wavelength measurements in the near-infrared (IR) region, the primary source of the pulses was an amplified erbium-doped fiber oscillator and a Ti:Sapphire regenerative amplifier, which was pumped by the frequency-doubled output of a Nd:YAG laser (CPA-2001, Clark, Dexter, MI) operating at a repetition rate of 1 kHz. The amplifier delivers pulses of sub-150 fs duration centered at 775 nm. The output of the amplifier is used to pump two tunable noncollinear parametric amplifiers (TOPAS White (Light Conversion) and NOPA (Clark)) to generate the pump (490 nm) and probe (900 nm) pulses used in the experiment. The intensity of excitation was ~5×10^{13} photons · pulse^{-1} · cm^{-2}. The experimental response function was measured to be 45 fs at the sample position by means of sum-frequency generation in a 30 μm beta barium borate (BBO) crystal. All single-wavelength measurements were carried out in a mode using two probe beams that overlapped with the excitation at the sample (one with parallel and the other with perpendicular polarization with respect to the excitation). The transient absorption signals of both polarizations were processed by data acquisition software (Pascher Instruments, Lund, Sweden). The values of isotropic (magic angle) and anisotropy signals were calculated from the parallel and perpendicular signals for each time point to obtain the kinetics of photogenerated population decay as well as orientation decay of the excitation-induced dipole, in addition to recorded kinetics with parallel and perpendicular polarizations. To minimize noise, a standard 1-mm quartz cuvette was used for the single-wavelength measurements. Test measurements comparing the kinetics obtained with rotating and standard cuvettes showed that, at the low excitation intensities used in these experiments, both cuvettes gave identical results, but a much better signal/noise ratio was achieved with the standard cuvette.

Data analysis

The kinetic traces collected by the diode-array detection system were fitted globally (DAFit, Pascher Instruments, Lund, Sweden). The data were fitted to a sum of exponentials, including numerical deconvolution of the full width at half-maximum of the response function, and a fourth-degree polynomial describing the chirp of the probe light. To visualize the excited-state dynamics, we used a model with time evolution according to a sequential, irreversible scheme: A→B, B→C…. The arrows represent increasingly slower monoexponential processes, and the time constants of these processes correspond to lifetimes of the species A, B, C, …. The spectral profiles of the species are called evolution-associated difference spectra (EADS) (31).

RESULTS

The absorption spectrum of xanthorhodopsin is shown in Fig. 1. It is dominated by the characteristic structure of the S_0-S_2 absorption band of the salinixanthin chromophore, which has vibrational peaks at 520, 486 and 458 nm. The retinal chromophore exhibits maximum absorbance around 560 nm. In methanol, salinixanthin shows a blue shift as compared with xanthorhodopsin, and only hints of vibrational peaks at 505, 477, and 447 nm. Treatment of xanthorhodopsin by $NaBH_4$ shifts the retinal band below 400 nm because it reduces the double bond of the retinal Schiff base to a single bond (20,32). Fig. 1 shows that the salinixanthin vibrational peaks are unchanged, a clear sign that the binding site remains intact, because its perturbation would significantly diminish the resolution of those peaks (22,33). The $NaBH_4$ treatment allows observation of excited-state dynamics when salinixanthin is specifically bound to the protein but in the absence of energy transfer.

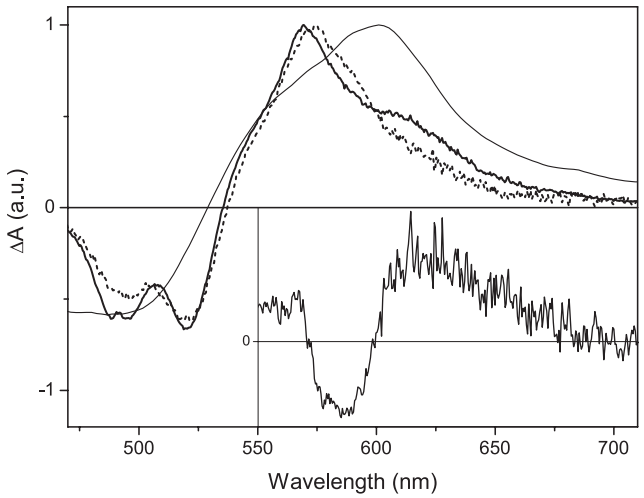

FIGURE 2 Transient absorption spectra for the untreated (*thick solid line*), $NaBH_4$-treated (*dashed line*) xanthorhodopsin, and salinixanthin in methanol (*thin solid line*) recorded at 1 ps after excitation at 490 nm. Spectra are normalized to maximum. (*Inset*) difference between transient spectra of untreated and $NaBH_4$-treated xanthorhodopsin in the 550–710 nm region.

Transient absorption in the visible region

To study energy transfer between salinixanthin and retinal, we excited xanthorhodopsin near the salinixanthin absorption maximum at 490 nm. Although the broad absorption band of the retinal chromophore extends well below 490 nm, salinixanthin has an ~5- to 6-fold larger extinction coefficient at this wavelength (20), and effects due to direct excitation of rhodopsin are therefore small. Transient absorption spectra taken at 1 ps after excitation are shown in Fig. 2. The $NaBH_4$-treated xanthorhodopsin exhibits features typical of a carotenoid. At 1 ps the S_2-S_1 internal conversion is finished and the excited-state absorption band, peaking at 574 nm, is due to the S_1-S_n transition of salinixanthin. The negative signal with two well-resolved bands at 520 and 490 nm reflects ground-state bleaching. Essentially the same features are observed in the transient absorption spectrum of salinixanthin in methanol, but the conformational disorder in solution makes the transient absorption spectrum significantly broader. The spectral features observed in the transient absorption spectrum of untreated xanthorhodopsin are similar to the $NaBH_4$-treated sample, but there is a clear increase of signal above 600 nm accompanied by a decrease of signal at ~580 nm. This is apparent from the difference between the transient absorption spectra of untreated and $NaBH_4$-treated xanthorhodopsin shown in the inset of Fig. 2. The spectrum is reminiscent of the J/K state of bacteriorhodopsin, indicating that energy transfer from

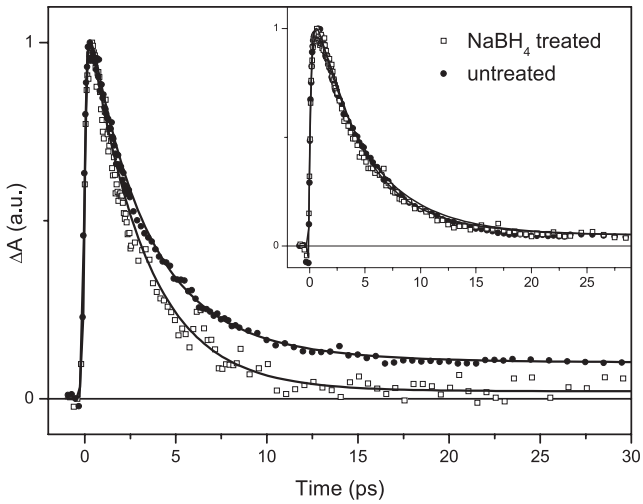

FIGURE 3 Kinetics recorded at 615 nm for $NaBH_4$-treated (*open symbols*) and untreated (*solid symbols*) xanthorhodopsin. (*Inset*) Kinetics at 560 nm. Solid lines are fits. Excitation wavelength was 490 nm.

salinixanthin initiated the xanthorhodopsin photocycle. Since the J state decays into the K state within a few picoseconds in the analogous protein, bacteriorhodopsin (15), the spectral feature observed at 1 ps in the untreated xanthorhodopsin must be mostly due to the J state, with some contribution from the K state.

The notion that energy is transferred from a state higher than S_1 is further corroborated by the kinetics measured at 615 nm, reflecting decay of the salinixanthin S_1 state (Fig. 3). Whereas for the $NaBH_4$-treated xanthorhodopsin there is no residual signal after 20 ps, formation of the K state of the photocycle is manifested as a nondecaying plateau in the untreated complex because the K-state lifetime is on a microsecond timescale (17,30). Fitting of the kinetics gives the same salinixanthin S_1 lifetime of 3 ps in both treated and untreated xanthorhodopsin, signaling that energy transfer does not proceed via the S_1 state of salinixanthin. The identical decays for the two complexes are best demonstrated at 560 nm, where there is no signal from the initial products of the photocycle (Fig. 3, *inset*). It must be noted, however, that the kinetics at 560 nm, both in the $NaBH_4$-treated and untreated samples, exhibit slower decay than the 3 ps extracted from fitting of the 615-nm kinetics, and cannot be fitted by a single-exponential decay. This is due to the so-called S* state that is identified from its distinct shoulder at the blue side of the S_1-S_n band.

To disentangle the contributions from various states, we applied global analysis to the data. The EADS extracted from global analysis are depicted in Fig. 4 for untreated and $NaBH_4$-treated xanthorhodopsin, and for salinixanthin in methanol. The initial EADS (*black curves*) represent a spectrum of the initially excited S_2 state of salinixanthin, which consists mainly of the ground-state bleaching and stimulated emission from the S_2 state. This spectrum decays in ~100 fs to form the second EADS (shown in *red*). This

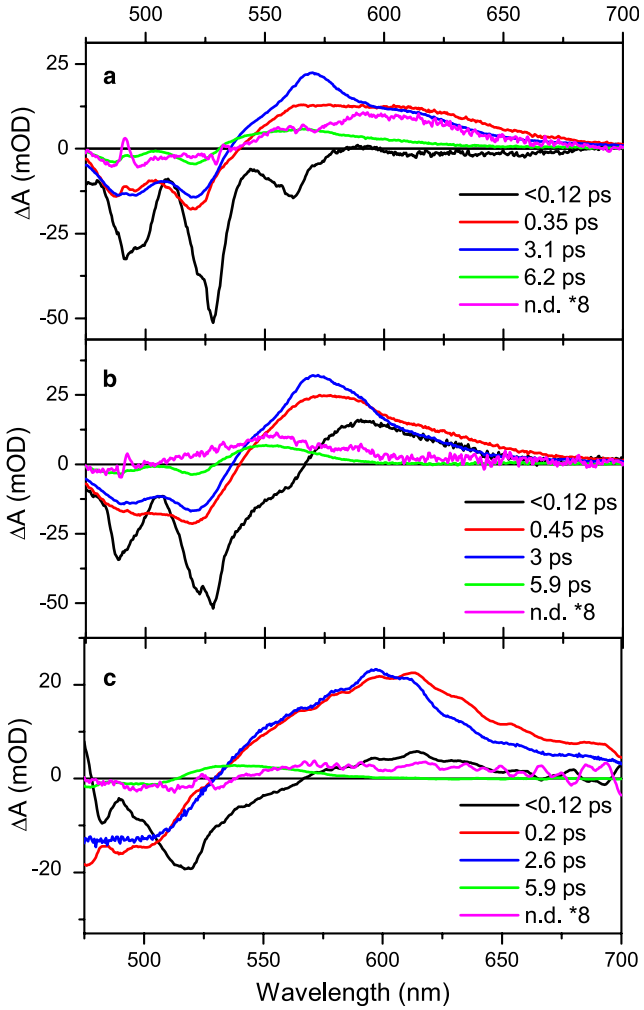

FIGURE 4 EADS from global fitting of data obtained after 490 nm excitation of untreated (*a*) and $NaBH_4$-treated (*b*) xanthorhodopsin compared with global fitting results of salinixanthin in methanol (*c*). The final, nondecaying (n.d.) EADS is multiplied by 8 in all panels.

spectrum has typical attributes of a hot S_1 state (34,35). The hot S_1 decays on a subpicosecond timescale to the relaxed S_1 state whose EADS are the blue curves in Fig. 4. The shoulder around 620 nm, which is clearly visible in this EADS for the untreated xanthorhodopsin, indicates that the J/K state of the photocycle has been also formed during this step. The S_1 EADS decays in 3 ps for the untreated and $NaBH_4$-treated xanthorhodopsin, whereas a slightly shorter lifetime, 2.6 ps, is obtained for salinixanthin in methanol. Moreover, to obtain good fits, all three samples require another EADS decaying with an ~6 ps time constant. The shape of this EADS is typical for the S* state (26). The final nondecaying EADS differs significantly for the three samples. In untreated xanthorhodopsin it has a broad feature centered at 610 nm ascribed to the K-state spectrum of the retinal chromophore. No long-lived photoproducts of retinal chromophore should be observed for $NaBH_4$-treated xanthorhodopsin, in which energy

transfer and direct excitation is prevented. However, global analysis gives a nondecaying (in the time domain of the experiment) spectrum even for the $NaBH_4$-treated xanthorhodopsin. This final EADS peaks at 550 nm and, based on comparison with other carotenoids, is ascribed to a triplet state of salinixanthin. The presence of a triplet state on the picosecond timescale is consistent with its ultrafast formation from the S* state by a homofission process (26,36). In fact, a hint of the triplet state could also be identified in the final EADS of the untreated xanthorhodopsin as a shoulder located at 560 nm (Fig. 4 *a*), indicating that the ultrafast triplet formation also occurs in untreated xanthorhodopsin. The final EADS of salinixanthin in methanol is featureless, indicating that the triplet formation by homofission is restricted to salinixanthin bound to the protein, in agreement with earlier observations in other carotenoid-containing systems (26,36,37).

Transient absorption in the near-IR region

Although the transient absorption measurements in the visible region give a clear indication of energy transfer from salinixanthin to the retinal chromophore, the time resolution of ~130 fs is not sufficient to obtain energy transfer rates. The lifetime of the S_2 state could be inferred from the lifetime of the first EADS, but since the S_2 lifetime of salinixanthin in the presence of energy transfer is expected to be on the sub-100 fs timescale (20), the limitation given by the time resolution precludes reliable assignment of the S_2 lifetime. Another complication in the visible spectral region arises from the overlapping contributions of various signals. The rise of the S_1-S_n band, for example, is not a good measure because it always contains a contribution from the S_1 vibrational relaxation as well (34,38).

Thus, to reliably determine the S_2 lifetime of salinixanthin, we used a femtosecond pump-probe setup with a time resolution of 40 fs. We chose 900 nm as a probing wavelength because at this wavelength carotenoids usually exhibit a strong S_2-S_n transition (39,40), and one can simultaneously monitor the appearance of the product of energy transfer, the excited retinal chromophore, that has a stimulated emission in the 800–950 nm region (41). The resulting kinetics are shown in Fig. 5 *a*. The instantaneous positive signal is due to the S_2-S_n transition. The initial decay can be fitted by a 110 fs time constant. The weak residual signal at longer delays is due to the S_1-S_2 transition that occurs for carotenoids in the 800–1800 nm spectral region (42,43). The lack of any negative signal attributable to the stimulated emission of rhodopsin confirms the absence of salinixanthin-to-retinal energy transfer in the $NaBH_4$-treated sample. Thus, the time constant of 110 fs obtained from fitting provides the intrinsic S_2 lifetime of salinixanthin in xanthorhodopsin. The kinetic trace obtained after the 490-nm excitation of untreated xanthorhodopsin clearly demonstrates energy transfer from salinixanthin to retinal. The initial decay of the S_2-S_n signal of

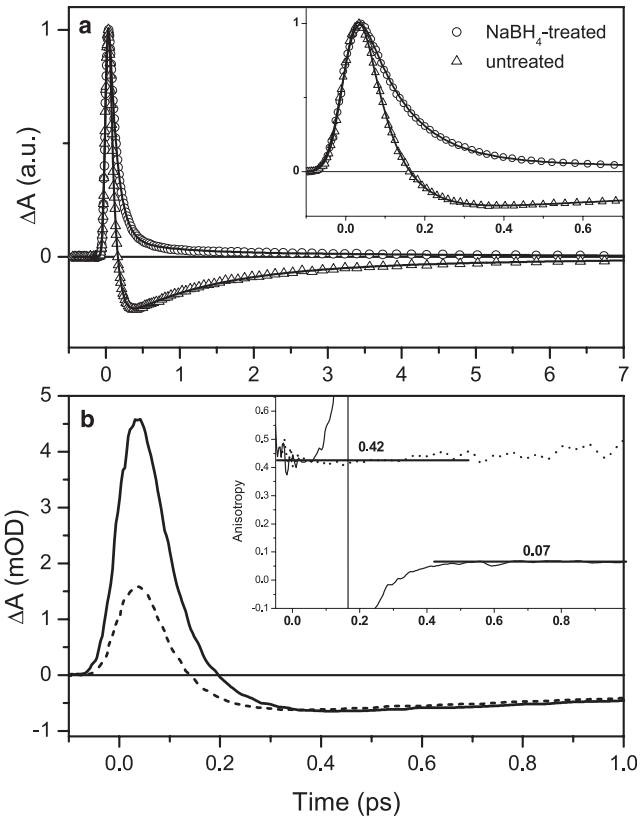

FIGURE 5 (*a*) Kinetics recorded at the maximum of stimulated emission of retinal chromophore, 900 nm, after excitation at 490 nm. Solid lines represent fits. (*Inset*) Enlargement of the initial part of the kinetics. (*b*) Kinetics measured at 900 nm for the untreated xanthorhodopsin with parallel (*solid*) and perpendicular (*dashed*) polarization with respect to the excitation at 490 nm. (*Inset*) Time evolution of anisotropy for untreated (*solid line*) and $NaBH_4$-treated (*dashed*) xanthorhodopsin.

salinixanthin produces a negative signal that is due to stimulated emission of the excited retinal.

Fitting the S_2-S_n decay with a single-exponential function gives a time constant of 70 fs, indicating that the S_2 lifetime is shortened because of energy transfer to rhodopsin. Detailed analysis of the samples demonstrated that the xanthorhodopsin used for these experiments contains 17% ± 3% of unbound salinixanthin (20). This means that the S_2-S_n decay should be double-exponential, with a minor component of ~110 fs reflecting the S_2 decay of the unbound salinixanthin. If we fix the second component to 110 fs and amplitude of 0.17, the major decay component corresponding to the S_2 lifetime of the bound salinixanthin becomes 62 fs. Letting all parameters free gives the major decay component of 64 fs and amplitude of 88%, whereas the second component has a time constant of 118 fs and amplitude of 12%. Based on this analysis, we conclude that the S_2 lifetime of the bound salinixianthin is in the 62–70 fs range. A mean value of 66 ± 4 fs is therefore used for calculation of the energy transfer rate (see the Discussion section). The stimulated emission of retinal

decays biexponentially, with time constants of 0.7 ps (64%) and 3.3 ps (36%), and thus more slowly than that of bacteriorhodopsin (41,44) (Fig. S5).

Energy transfer between salinixanthin and the retinal chromophore can be further explored by measuring anisotropy decay. Kinetics for the untreated xanthorhodopsin excited at 490 nm recorded for parallel and perpendicular polarization between the pump and probe beams are shown, along with resulting anisotropy decay, in Fig. 5 *b*. Although the fact that the kinetics change sign prevents fitting of the anisotropy decay, it is obvious that the initial anisotropy of 0.42 decays during the first 400 fs to its final value of 0.07. Using the equation (45)

$$r = 0.2\left(3\cos^2\alpha - 1\right)$$

for calculation, the angle α between the transition dipole moments of donor and acceptor from the final anisotropy r gives an angle of 48°, matching the value of 46° obtained from the xanthorhodopsin structure (21) for the angle between molecular axes of salinixanthin and retinal. It should be noted, however, that it is only an approximation because it ignores a small contribution from direct excitation of the retinal chromophore at 490 nm. Since anisotropy measured for the $NaBH_4$-treated xanthorhodopsin does not exhibit any decay during the first few picoseconds (Fig. 5b, *inset*), time-resolved anisotropy further corroborates the S_2-mediated energy transfer from salinixanthin to retinal.

DISCUSSION

Previous studies of xanthorhodopsin demonstrated salinixanthin-to-retinal energy transfer from action spectra of inhibition of respiration (17) and from fluorescence excitation spectra (20). In our attempts to resolve the energy transfer pathway(s) and quantify the energy transfer efficiency, the excited-state properties in the absence of energy transfer provide important input information. Although for many carotenoid-(bacterio)chlorophyll photosynthetic antennae it is feasible to approximate excited-state properties of the carotenoid bound to a protein with those observed in solution (2), this approximation is inadequate for salinixanthin. Salinixanthin is a carotenoid with a complicated structure (Supporting Material) and it contains a conjugated carbonyl group that is known to make the excited-state properties dependent on the polarity of the environment (27–29). Moreover, the absorption spectrum of salinixanthin in solution differs markedly from that in xanthorhodopsin (Fig. 2): the clearly pronounced vibrational peaks in xanthorhodopsin indicate a specific locked conformation of salinixanthin when bound to protein. A comparable change of the absorption spectrum upon binding was observed for a similar carotenoid, hydroxyechinenone, resulting in a significant reduction of the lifetime of the lowest excited state (46,47).

Effect of the binding site on salinixanthin excited-state properties

The significant increase in the resolution of vibrational bands of the S_0-S_2 transition induced by binding to the protein indicates a well-defined binding site that locks a specific carotenoid conformation (21). In solution, the long conjugated backbone allows for a distribution of conformers, resulting in loss of vibrational structure. Enhanced resolution of the vibrational bands was previously reported even for shorter carotenoids upon binding to light-harvesting proteins (48) or the orange carotenoid protein (OCP) (46), but the increase in resolution of vibrational bands upon binding is the largest in xanthorhodopsin.

Binding of salinixanthin in xanthorhodopsin also induces a red shift of the salinixanthin absorption bands compared to methanol. This shift is a marker of a carotenoid-protein interaction. In xanthorhodopsin, however, the magnitude of the red shift, ~550 cm^{-1}, is significantly less than in other carotenoid-protein systems whose protein-induced red shift often reaches 1000 cm^{-1} (48). Although this may indicate a weaker interaction between salinixanthin and its binding site in xanthorhodopsin, the high-resolution structure (21) offers another explanation. The dihedral angle between the conjugated terminal ring and the main conjugated backbone is 82° (21), making the ring nearly perpendicular to the plane of the main conjugation. In solution, the planes of the terminal ring and the main conjugation are twisted by ~40° due to repulsion between the methyl groups on the ring and the hydrogen atoms on the conjugated backbone (49). Because this twist is known to decrease the effective conjugation length as compared with linear carotenoids (2), the larger dihedral angle in xanthorhodopsin should result in a shorter effective conjugation length of salinixanthin when locked in the binding site. This causes a blue shift of absorption bands, thus diminishing the overall protein-induced red shift of absorption bands resulting from the salinixanthin-protein interaction.

The decrease of the effective conjugation length induced by binding would also affect the S_1 lifetime. Indeed, in solution it is 2.6 ps, whereas an S_1 lifetime of 3.1 ps is obtained for salinixanthin in $NaBH_4$-treated xanthorhodopsin. When we compare these lifetimes with those obtained for various linear carotenoids (see Table 3 in Polívka and Sundström (2)), we see that the S_1 lifetime of 2.6 ps corresponds to the effective conjugation $N_{eff} \sim 12$. Consequently, although salinixanthin has a total of 13 conjugated double bonds, the twisting of the terminal ring and *s-cis* orientation of the double bonds at the ring makes the effective conjugation shorter. The lifetime of 3.1 ps in the protein indicates further shortening to $N_{eff} \sim 11.5$ caused by increasing the dihedral angle between the terminal ring and the main conjugation.

We should also examine the possible effect of the ICT state, because enhancement of the ICT state effect was

observed upon binding of a carotenoid with a similar conjugated backbone, hydroxyechinenone, to a different carotenoid-binding protein, OCP (46). In solution, both salinixanthin and hydroxyechinenone exhibit only minor polarity-induced effects, as expected for carbonyl carotenoids with a long conjugation (27–29). Both absorption and transient absorption spectra show only mild asymmetric broadening when the solvent is changed from *n*-hexane to methanol (46) (Supporting Material), and the S_1 lifetime remains unaffected by solvent polarity. In OCP the binding site clearly stabilizes the ICT state of hydroxyechinenone (46,47). In contrast, no spectral bands attributable to the ICT state are observed in xanthorhodopsin. The difference in stabilization of the ICT state is obvious from the structures of the two binding sites. Whereas OCP stretches the carotenoid in a way that makes the conjugated carbonyl group linear and planarized with the rest of the conjugation (50), xanthorhodopsin isolates the terminal ring containing the conjugated carbonyl group by twisting the ring significantly out of the main conjugation plane (21).

Salinixanthin to retinal energy transfer

Previous studies unequivocally proved that salinixanthin transfers energy to retinal (17,20,51). The identical S_1 lifetimes for untreated and $NaBH_4$-treated xanthorhodopsin show that no energy transfer channel operates via the S_1 state of salinixanthin. The absence of S_1-mediated energy transfer is in agreement with the fact that the S_1 state of a carotenoid with N_{eff} ~11.5 is expected to have an energy lower than 13,000 cm^{-1} (2,24), thus more than 4000 cm^{-1} below the lowest excited state of retinal chromophore (20).

Thus, the major energy transfer channel proceeds via the S_2 state of salinixanthin, in agreement with the conclusion drawn from a previous steady-state fluorescence study (20). The activity of this channel is clearly demonstrated by the different S_2 lifetimes of salinixanthin in untreated and $NaBH_4$-treated xanthorhodopsin. The intrinsic (without energy transfer) S_2 lifetime $\tau_{S2} = 110$ fs is obtained for $NaBH_4$-treated xanthorhodopsin, and it is shortened to $\tau_{XR} = 66 \pm 4$ fs because of an additional depopulation pathway, the energy transfer to retinal. The measured salinixanthin S_2 lifetime of 66 fs in xanthorhodopsin confirms the value estimated from the S_2 fluorescence emission quantum yield (20). The energy transfer time τ_{ET} is then calculated as $\tau_{ET} = (1/\tau_{XR} - 1/\tau_{S2})^{-1} = 165 \pm 25$ fs, and the resulting efficiency of the S_2-mediated energy transfer is 40% ± 4%. The obtained value falls into the range of 33–45% determined for total salinixanthin to retinal energy transfer either from action spectra of inhibition of respiration (17,51) or fluorescence excitation spectra (20).

The energy transfer rate k_{ET} (in ps^{-1}) can be calculated according to the following equation (52):

$$k_{ET} = 1.18V^2\Theta,$$

where V is the interaction term and Θ is the spectral overlap integral given by

$$\Theta = \int \frac{F(\nu)A(\nu)}{\nu^4} d\nu,$$

where $F(\nu)$ and $A(\nu)$ represent emission spectrum of the donor and absorption spectrum of the acceptor, both converted to the energy scale and normalized to the unit area (52). The overlap integral yields values of 1.33–1.77 × 10^{-4}, depending on whether we use the measured salinixanthin S_2 emission or the mirror image of the absorption spectrum (see curves 2 and 3 in Fig. 3 *c* of Balashov et al. (20)). Thus, using the experimentally determined energy transfer rate of $(0.165 \pm 0.025\ ps)^{-1}$, we obtain a range of V ~ 160–210 cm^{-1}, a value comparable with carotenoid-bacteriochlorophyll antenna systems that also utilize the S_2 pathway (53).

As discussed above, the S_1 and/or ICT states cannot be the donors because of their low energy; however, earlier theoretical works (54) and experimental studies in the last decade revealed that other dark states, $1B_u^-$ and $3A_g^-$, may be located between the S_2 and S_1 states for carotenoids with conjugation lengths $N > 10$ (2,24). Experimental values obtained from resonance Raman profiles put the $1B_u^-$ state below 16,000 cm^{-1} for a carotenoid with $N_{eff} = 11.5$ (24), and thus significantly below the lowest excited state of retinal in xanthorhodopsin. Even if the $1B_u^-$ state were high enough to achieve appreciable spectral overlap, its dipole moment should be ~2 orders of magnitude lower than that of the S_2 state (55), making the coupling to retinal negligible. The weak coupling and expected short $1B_u^-$ lifetime of 80–300 fs (24) rule out this state as a significant additional energy donor in salinixanthin-retinal energy transfer. The same analysis holds also for the $3A_g^-$ state. Its expected location above the $1B_u^-$ state may generate reasonable spectral overlap, but its negligible dipole moment and short lifetime prevents this state from playing a role in energy transfer.

The S* state and triplet formation

Global fitting reveals that another excited state, S*, is involved in the excited-state dynamics of salinixanthin. EADS decaying with ~6 ps have typical attributes of the S* state (26,36). In solution, the magnitude of the S* band in the 5.9 ps EADS does not exceed 10% of the maximum of the S_1-S_N band (Fig. 4 *c*). The magnitude of the S* band obtained here indicates that the S* state is populated from the S_2 state with <10% efficiency, assuming that the ratio of the oscillator strengths of the S*-S_N and S_1-S_n transitions of salinixanthin is ~0.8, the value from target analysis of transient data taken for spirilloxanthin (26) or spheroidene (36). The S* formation is more efficient when salinixanthin is locked in the xanthorhodopsin-binding site, where an upper limit of 20% can be inferred from analysis of EADS. Since the S* state was recently identified as the S_1 state of carotenoids with

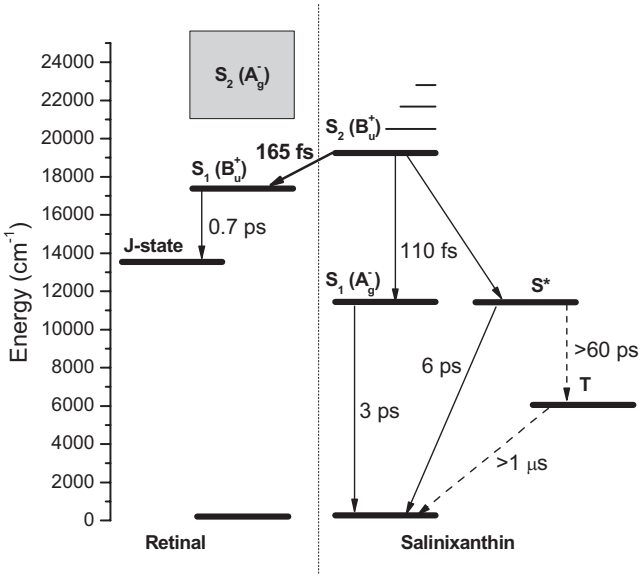

FIGURE 6 Energy-level diagram depicting relaxation processes that occur after excitation of the S_2 state of salinixanthin in xanthorhodopsin. The thick solid arrow represents the energy transfer channel, and the thin solid arrows correspond to the main intramolecular relaxation processes. The dashed lines represent processes involving the salinixanthin triplet state. The processes described in this study are labeled by corresponding time constants. The S* to triplet conversion is depicted only schematically because the homofission process first forms a doubly excited triplet that is isoenergetic with the S* state, which then relaxes to the lowest triplet state (26,36). The >60 ps time constant obtained from the estimated branching ratio represents the total time for this two-step process. The lifetime of the triplet was not measured in this study and the >1 μs time constant is a rough estimate based on knowledge of carotenoid triplet lifetimes in other systems. The dotted line represents the first step in the xanthorhodopsin photocycle, formation of the J state from the excited retinal chromophore (only the major component is shown, see text for details). Since the energy of the J state is not known, it is only schematically placed above the 11.6 $\pm$ 3.4 kcal/mol determined for the K state of bacteriorhodopsin (59). The energy of the forbidden S_2 state of retinal in xanthorhodopsin has not been determined. The expected range from studies of bacteriorhodopsin (60) and protonated Schiff bases of retinal (61) is shown in gray. Vibrational bands of the salinixanthin S_2 state are depicted to demonstrate that excitation at 490 nm (the 0–1 transition) is somewhat below the lowest expected S_2 energy of retinal in xanthorhodopsin. This and the low oscillator strength of the S_2 state of retinal would seem to preclude a significant involvement of this state in energy transfer.

excited-state conformation deviating from the ideal all-*trans* conformation (35,56), this increase is most likely due to a deformation of the conjugated chain of salinixanthin that takes a ''wavy'' shape in the binding site (21).

An important difference between the salinixanthin S* state in solution and in xanthorhodopsin is triplet formation. Whereas in solution the S* state decays exclusively to the ground state, in the $NaBH_4$-treated xanthorhodopsin the final, nondecaying EADS contains a weak band peaking at ~550 nm that is characteristic of the T_1-T_N transition of carotenoids (57). Thus, when salinixanthin is bound to the protein, the S* state serves as a precursor of ultrafast triplet formation by homofission, a process described previously for other carotenoids bound to some light-harvesting proteins. However, a comparison of the magnitudes of the carotenoid triplet bands obtained here with those of the light-harvesting proteins shows that the efficiency of the triplet yield is much lower in xanthorhodopsin. Although up to 30% of the S* population is converted to the triplet state in light-harvesting proteins of purple bacteria (26,36), the intensity of the triplet band in xanthorhodopsin suggests that <10% of the S* population is converted. Also, in contrast to some purple bacterial light-harvesting systems (36,58), no energy transfer from the S* state was found in xanthorhodopsin. The identified relaxation pathways are depicted in Fig. 6.

SUPPORTING MATERIAL

Methods, five figures, and references are available at http://www.biophysj.org/biophysj/supplemental/S0006-3495(09)00380-4.

Research in the Czech Republic was supported by grants from the Czech Ministry of Education (MSM6007665808 and AV0Z50510513) and the grant agency of the Czech Academy of Sciences (IAA608170604). T.P. received financial support from the Access to Research Infrastructures Activity in the Sixth Framework Program of the European Union (212025 Laserlab-Europe Cont.) for conducting part of the research in Lund. The work at Lund University was supported by grants from the Swedish Research Council and the Wallenberg Foundation. The UCI group was supported in part by grants from the U.S. Army Research Office (W911NF-06-1-0020 to S.P.B. and J.K.L.), the National Institutes of Health (GM29498), and the Department of Energy (DEFG03-86ER13525 to J.K.L.).

REFERENCES

1. Green, R. B., and W. W. Parson, editors. (2003). Light-Harvesting Antennas in Photosynthesis. Kluwer, Dordrecht, The Netherlands.
2. Polívka, T., and V. Sundström. 2004. Ultrafast dynamics of carotenoid excited states—from solution to natural and artificial systems. *Chem. Rev.* 104:2021–2071.
3. Ritz, T., A. Damjanovic, K. Schulten, J. P. Zhang, and Y. Koyama. 2000. Efficient light harvesting through carotenoids. *Photosynth. Res.* 66:125–144.
4. van Amerongen, H., and R. van Grondelle. 2001. Understanding the energy transfer function of LHCII, the major light-harvesting complex of green plants. *J. Phys. Chem. B.* 105:604–617.
5. Polívka, T., R. G. Hiller, and H. A. Frank. 2007. Spectroscopy of the peridinin – chlorophyll-a protein: insight into light-harvesting strategy of marine algae. *Arch. Biochem. Biophys.* 458:111–120.
6. Mathies, R. A., S. W. Lin, J. B. Ames, and W. T. Pollard. 1991. From femtoseconds to biology: mechanism of bacteriorhodopsin's light-driven proton pump. *Annu. Rev. Biophys. Biophys. Chem.* 20:491–518.
7. Balashov, S. P. 2000. Protonation reactions and their coupling in bacteriorhodopsin. *Biochim. Biophys. Acta.* 1460:75–94.
8. Lanyi, J., and B. Schobert. 2004. Local-global conformational coupling in a heptahelical membrane protein: transport mechanism from crystal structures of the nine states in the bacteriorhodopsin photocycle. *Biochemistry.* 43:3–8.
9. Subramaniam, S., T. Hirai, and R. Henderson. 2002. From structure to mechanism: electron crystallographic studies of bacteriorhodopsin. *Philos. Trans. R. Soc. Lond. A.* 360:859–874.
10. Kobayashi, T., T. Saito, and H. Ohtani. 2001. Real-time spectroscopy of transition states of bacteriorhodopsin during retinal isomerization. *Nature.* 414:531–534.

11. Sharkov, A. V., A. V. Pakulev, S. V. Chekalin, and Y. A. Matveetz. 1985. Primary events in bacteriorhodopsin probed by subpicosecond spectroscopy. *Biochim. Biophys. Acta*. 808:94–102.
12. Kahan, A., O. Nahmias, N. Friedman, M. Sheves, and S. Ruhman. 2007. Following photoinduced dynamics in bacteriorhodopsin with 7-fs impulsive vibrational spectroscopy. *J. Am. Chem. Soc*. 129: 537–546.
13. Herbst, J., K. Heyne, and R. Diller. 2002. Femtosecond infrared spectroscopy of bacteriorhodopsin chromophore isomerization. *Science*. 297:822–825.
14. Gai, F., K. C. Hasson, J. C. McDonald, and P. A. Anfinrud. 1998. Chemical dynamics in proteins: the photoisomerization of retinal in bacteriorhodopsin. *Science*. 279:1886–1891.
15. Kochendoerfer, G. G., and R. A. Mathies. 1995. Ultrafast spectroscopy of rhodopsins—photochemistry at its best. *Isr. J. Chem*. 35:211–226.
16. Fuhrman, J. A., M. S. Schwalbach, and U. Stingl. 2008. Proteorhodopsins: an array of physiological roles? *Nat. Rev. Microbiol*. 6:488–494.
17. Balashov, S. P., E. S. Imasheva, V. A. Boichenko, J. Antón, J. M. Wang, et al. 2005. Xanthorhodopsin: a proton pump with a light-harvesting carotenoid antenna. *Science*. 309:2061–2064.
18. Antón, J., A. Oren, S. Benlloch, F. Rodríguez-Valera, R. Amann, et al. 2002. *Salinibacter ruber* gen. nov., sp. nov., a novel, extremely halophilic member of the *Bacteria* from saltern crystallizer ponds. *Int. J. Syst. Evol. Microbiol*. 52:485–491.
19. Lutnaes, B. F., A. Oren, and S. Liaaen-Jensen. 2002. New C_{40}-carotenoid acyl glycoside as principal carotenoid in *Salinibacter ruber*, an extremely halophilic eubacterium. *J. Nat. Prod*. 65:1340–1343.
20. Balashov, S. P., E. S. Imasheva, J. M. Wang, and J. K. Lanyi. 2008. Excitation energy transfer and the relative orientation of retinal and carotenoid in xanthorhodopsin. *Biophys. J*. 95:2402–2414.
21. Luecke, H., B. Schobert, J. Stagno, E. S. Imasheva, J. M. Wang, et al. 2008. Crystallographic structure of xanthorhodopsin, the light-driven proton pump with a dual chromophore. *Proc. Natl. Acad. Sci. USA*. 105:16561–16565.
22. Imasheva, E. S., S. P. Balashov, J. M. Wang, E. Smolensky, M. Sheves, et al. 2008. Chromophore interaction in xanthorhodopsin—retinal dependence of salinixanthin binding. *Photochem. Photobiol*. 84: 977–984.
23. Cong, H., D. M. Niedzwiedzki, G. N. Gibson, A. M. LaFountain, R. M. Kelsh, et al. 2008. Ultrafast time-resolved carotenoid-to-bacteriochlorophyll energy transfer in LH2 complexes from photosynthetic bacteria. *J. Phys. Chem. B*. 112:10689–10703.
24. Koyama, Y., F. S. Rondonuwu, R. Fujii, and Y. Watanabe. 2004. Light-harvesting function of carotenoids in photosynthesis: the roles of the newly found $1B_u^-$ state. *Biopolymers*. 74:2–18.
25. Marian, C. M., and N. Gilka. 2008. Performance of the density functional theory/multireference configuration interaction method on electronic excitation of extended π-systems. *J. Chem. Theory Comput*. 4:1501–1515.
26. Gradinaru, C. C., J. T. M. Kennis, E. Papagiannakis, I. H. M. van Stokkum, R. J. Cogdell, et al. 2001. An unusual pathway of excitation energy deactivation in carotenoids: singlet-to-triplet conversion on an ultrafast timescale in a photosynthetic antenna. *Proc. Natl. Acad. Sci. USA*. 98:2364–2369.
27. Frank, H. A., J. A. Bautista, J. Josue, Z. Pendon, R. G. Hiller, et al. 2000. Effect of the solvent environment on the spectroscopic properties and dynamics of the lowest excited states of carotenoids. *J. Phys. Chem. B*. 104:4569–4577.
28. Zigmantas, D., R. G. Hiller, F. P. Sharples, H. A. Frank, V. Sundström, et al. 2004. Effect of a conjugated carbonyl group on the photophysical properties of carotenoids. *Phys. Chem. Chem. Phys*. 6:3009–3016.
29. Stalke, S., D. A. Wild, T. Lenzer, M. Kopczynski, P. W. Lohse, et al. 2008. Solvent-dependent ultrafast internal conversion dynamics of n′-apo-β-*carotenoic*-n′-acids (n=8, 10, 12). *Phys. Chem. Chem. Phys*. 10:2180–2188.
30. Imasheva, E. S., S. P. Balashov, J. M. Wang, and J. K. Lanyi. 2006. pH-dependent transitions in xanthorhodopsin. *Photochem. Photobiol*. 82:1406–1413.
31. van Stokkum, I. H. M., D. S. Larsen, and R. van Grondelle. 2004. Global and target analysis of time-resolved spectra. *Biochim. Biophys. Acta*. 1657:82–104.
32. Peters, J., R. Peters, and W. Stoeckenius. 1976. A photosensitive product of sodium borohydride reduction of bacteriorhodopsin. *FEBS Lett*. 61:128–134.
33. Balashov, S. P., E. S. Imasheva, and J. K. Lanyi. 2006. Induced chirality of light-harvesting carotenoid salinixanthin and its interaction with the retinal of xanthorhodopsin. *Biochemistry*. 45:10998–11004.
34. de Weerd, F. L., I. H. M. van Stokkum, and R. van Grondelle. 2002. Subpicosecond dynamics in the excited state absorption of all-*trans*-β-carotene. *Chem. Phys. Lett*. 354:38–43.
35. Niedzwiedzki, D., J. F. Koscielecki, H. Cong, J. O. Sullivan, G. N. Gibson, et al. 2007. Ultrafast dynamics and excited state spectra of open-chain carotenoids at room and low temperatures. *J. Phys. Chem. B*. 111:5984–5998.
36. Papagiannakis, E., J. T. M. Kennis, I. H. M. van Stokkum, R. J. Cogdell, and R. van Grondelle. 2002. An alternative carotenoid-to-bacteriochlorophyll energy transfer pathway in photosynthetic light harvesting. *Proc. Natl. Acad. Sci. USA*. 99:6017–6022.
37. Papagiannakis, E., I. H. M. van Stokkum, M. Vengris, R. J. Cogdell, R. van Grondelle, et al. 2006. Excited-state dynamics of carotenoids in light-harvesting complexes. 1. Exploring the relationship between the S_1 and S* states. *J. Phys. Chem. B*. 110:5727–5736.
38. Billsten, H. H., D. Zigmantas, V. Sundström, and T. Polívka. 2002. Dynamics of vibrational relaxation in the S_1 state of carotenoids having 11 conjugated C=C bonds. *Chem. Phys. Lett*. 355:465–470.
39. Papagiannakis, E., I. H. M. van Stokkum, R. van Grondelle, R. A. Niederman, D. Zigmantas, et al. 2003. A near-infrared transient absorption study of the excited-state dynamics of the carotenoid spirilloxanthin in solution and in the LH1 complex of *Rhodospirillum rubrum*. *J. Phys. Chem. B*. 107:11216–11223.
40. Zhang, J. P., L. H. Skibsted, R. Fujii, and Y. Koyama. 2001. Transient absorption from the $1B_u^+$ state of all-*trans*-β-carotene newly identified in the near-infrared region. *Photochem. Photobiol*. 73:219–222.
41. McCamant, D. W., P. Kukura, and R. A. Mathies. 2005. Femtosecond stimulated Raman study of excited-state evolution in bacteriorhodopsin. *J. Phys. Chem. B*. 109:10449–10457.
42. Polívka, T., J. L. Herek, D. Zigmantas, H. E. Åkerlund, and V. Sundström. 1999. Direct observation of the (forbidden) S_1 state in carotenoids. *Proc. Natl. Acad. Sci. USA*. 96:4914–4917.
43. Polívka, T., D. Zigmantas, H. A. Frank, J. A. Bautista, J. L. Herek, et al. 2001. Near-infrared time-resolved study of the S_1 state dynamics of the carotenoid spheroidene. *J. Phys. Chem. B*. 105:1072–1080.
44. Kennis, J. T. M., D. S. Larsen, K. Ohta, M. T. Facciotti, R. M. Glaeser, et al. 2002. Ultrafast protein dynamics of bacteriorhodopsin probed by photon echo and transient absorption spectroscopy. *J. Phys. Chem. B*. 106:6067–6080.
45. Lakowicz, J. R. 2006. Principles of Fluorescence Spectroscopy. Springer, Singapore.
46. Polívka, T., C. A. Kerfeld, T. Pascher, and V. Sundström. 2005. Spectroscopic properties of the carotenoid 3′-hydroxyechinenone in the orange carotenoid protein from the cyanobacterium. *Arthrospira maxima*. *Biochemistry*. 44:3994–4003.
47. Wilson, A., C. Punginelli, A. Gall, C. Bonetti, M. Alexandre, et al. 2008. A photoactive carotenoid protein acting as light intensity sensor. *Proc. Natl. Acad. Sci. USA*. 105:12075–12080.
48. Polívka, T., D. Zigmantas, J. L. Herek, Z. He, T. Pascher, et al. 2002. The carotenoid S_1 state in LH2 complexes from purple bacteria *Rhodobacter sphaeroides* and *Rhodopseudomonas acidophila*: S_1 energies, dynamics, and carotenoid radical formation. *J. Phys. Chem. B*. 106:11016–11025.

49. Schlucker, S., A. Szeghalmi, M. Schmitt, J. Popp, and W. Kiefer. 2003. Density functional and vibrational spectroscopic analysis of β-carotene. *J. Raman Spectrosc.* 34:413–419.

50. Kerfeld, C. A., M. R. Sawaya, V. Brahmandam, D. Cascio, K. K. Ho, et al. 2003. The crystal structure of a cyanobacterial water-soluble carotenoid binding protein. *Structure*. 11:55–65.

51. Boichenko, V. A., J. M. Wang, J. Antón, J. K. Lanyi, and S. P. Balashov. 2006. Functions of carotenoids in xanthorhodopsin and archaerhodopsin, from action spectra of photoinhibition of cell respiration. *Biochim. Biophys. Acta.* 1757:1649–1656.

52. Pullerits, T., S. Hess, J. L. Herek, and V. Sundström. 1997. Temperature dependence of excitation transfer in LH2 of. *Rhodobacter sphaeroides*. *J. Phys. Chem. B*. 101:10560–10567.

53. Krueger, B. P., G. D. Scholes, and G. R. Fleming. 1998. Calculation of couplings and energy-transfer pathways between the pigments of LH2 by the ab initio transition density cube method. *J. Phys. Chem. B*. 102:5378–5386.

54. Tavan, P., and K. Schulten. 1986. The low-lying electronic excitations in long polyenes—a PPP-MRD-CI study. *J. Chem. Phys.* 85:6602–6609.

55. Ghosh, D., J. Hachmann, T. Yanai, and G. K. L. Chan. 2008. Orbital optimization in the density matrix renormalization group, with applications to polyenes and β-carotene. *J. Chem. Phys.* 128:144117.

56. Niedzwiedzki, D. M., J. O. Sullivan, T. Polívka, R. R. Birge, and H. A. Frank. 2006. Femtosecond time-resolved transient absorption spectroscopy of xanthophylls. *J. Phys. Chem. B*. 110:22872–22885.

57. Fujii, R., K. Furuichi, J. P. Zhang, H. Nagae, H. Hashimoto, et al. 2002. Cis-to-*trans* isomerization of spheroidene in the triplet state as detected by time-resolved absorption spectroscopy. *J. Phys. Chem. A*. 106: 2410–2421.

58. Wohlleben, W., T. Buckup, J. L. Herek, R. J. Cogdell, and M. Motzkus. 2003. Multichannel carotenoid deactivation in photosynthetic light harvesting as identified by an evolutionary target analysis. *Biophys. J.* 85:442–450.

59. Birge, R. R., T. M. Cooper, A. F. Lawrence, M. B. Masthay, C. F. Zhang, et al. 1991. Revised assignment of energy storage in the primary photochemical event in bacteriorbodopsin. *J. Am. Chem. Soc.* 113:4327–4328.

60. Birge, R. R., and C. F. Zhang. 1990. Two-photon double resonance spectroscopy of bacteriorhodopsin. Assignment of the electronic and dipolar properties of the low-lying ^1A_g-like $1B_u^+$-like π, π^* states. *J. Chem. Phys.* 92:7179–7195.

61. Nielsen, I. B., L. Lammich, and L. H. Andersen. 2006. S_1 and S_2 excited states of gas-phase Schiff-base retinal chromophores. *Phys. Rev. Lett.* 96, 018304.